Bulletin of the Seismological Society of America, Vol. 94, No. 1, pp. 117–130, February 2004

The 27 May 1995 M_s 7.6 Northern Sakhalin Earthquake: An Earthquake on an Uncertain Plate Boundary

by Kei Katsumata, Minoru Kasahara, Masayoshi Ichiyanagi, Masayuki Kikuchi, Rak-Se Sen, Chun-Un Kim, Alexei Ivaschenko, and Ruben Tatevossian

Abstract On 27 May 1995, a large earthquake (M_s 7.6) occurred in the northern part of Sakhalin Island near an uncertain plate boundary between the Okhotsk (or the North American) plate and the Eurasian (or the Amurian) plate. The source process of the mainshock, the detailed aftershock activity, the *b*-value of the frequency–magnitude relationship for aftershocks, and the 3D *P*-wave velocity distribution have been investigated. Thirty-one body-wave records were inverted to determine the sequence of subevents of the mainshock using an iterative deconvolution method. The source parameters obtained are the location of the initial epicenter (52.64° N, 142.83° E); the centroid depth (9 km); strike, dip, and slip, equal to (191°, 87°, −172°) for the first subevent, (198°, 76°, −175°) for a second subevent, and (196°, 79°, −174°) for the combined source; and the total seismic moment M_0 (4.2×10^{19} N m) and M_w (7.0). We also deployed 12 temporary seismographic stations in the focal area from 7 June to 8 July 1995. More than 2000 events were located in an aftershock area of 60 km × 10 km that trends in a N15°E direction, which is consistent with the location of the surface rupture tracing the Gyrgylan'i–Ossoy fault. The *P*-wave velocity patterns were compared with the aftershock seismicity and the spatial distribution of the *b*-values, with results suggesting that high velocity correlates with high seismicity and small *b*-value. Our research strongly suggests that the 1995 Sakhalin earthquake was one of the outstanding events that define the uncertain plate boundary.

Introduction

On 27 May 1995, an earthquake with magnitude M_s 7.6 occurred in the northern part of Sakhalin Island (Arefiev *et al.*, 2000). Seventeen five-story apartment buildings collapsed in the town of Neftegorsk, and more than 2000 people were killed. The length of the surface fault ruptured by the mainshock was approximately 35 km, and the maximum displacement along the fault was approximately 7 m (Shimamoto *et al.*, 1996). Coseismic crustal deformation was also clearly detected by a Global Positioning System (GPS) network (Takahashi *et al.*, 1995) and by synthetic aperture radar interferometry (Tobita *et al.*, 1998).

What caused the large earthquake in this region? Although the microearthquake seismicity was relatively high before this earthquake, historical earthquakes larger than *M* 7.0 were not known in the northern part of Sakhalin Island (Solov'yev, 1965; Ivashchenko *et al.*, 1990; Kim, 1990; Kim and Bondarenko, 1990). Geologists had previously traced the Gyrgylan'i–Ossoy fault in northern Sakhalin (Fournier *et al.*, 1994), and the surface rupture coincided with this fault. Therefore the damaging strong ground motions were probably due to the rupture of this fault.

What loaded the tectonic stress on this fault? The plate boundary is a clue to understanding the answer to this question. A boundary between the Eurasian (or the Amurian) plate and the Okhotsk (or the North American) plate is supposed to run from north to south along Sakhalin Island (Chapman and Solomon, 1976; Seno *et al.*, 1996) (Fig. 1). Seismicity is the primary basis for identifying the plate boundary. There are many shallow microearthquakes on Sakhalin Island, and the north–south–trending seismic belt is about 300 km wide. Chapman and Solomon (1976) briefly reviewed the recent tectonics in Sakhalin Island as follows: "Sakhalin Island is dominated structurally by compressive features such as faults and folds that trend north–south along the longitudinal axis of the island. One of the primary faults is the central Sakhalin fault, a thrust fault with a meridional trend and a westerly dip of approximately 70°. The strike of drag folds and second-order faults indicate some right lateral movement along the main fault. This fault is dated as being active in the late Miocene and Pliocene, and it is still active today (Zanyukov, 1971). Quaternary displacements have been measured, and the epicenters of crustal earthquakes are

located in the fault zone." Based on the seismicity and the recent tectonics, Chapman and Solomon (1976) proposed that the plate boundary runs on Sakhalin Island from north to south.

The 1995 northern Sakhalin earthquake probably occurred on this uncertain plate boundary, suggesting that the Eurasian–Okhotsk plate boundary model is correct. To further the understanding of this plate boundary, we investigate and describe in detail the recent earthquake sequence.

The components of this article include the study of the source process of the mainshock using broadband seismograms from the Incorporated Research Institutions for Seismology (IRIS) data center, the spatial and temporal distributions of aftershocks using travel-time data from temporary local seismic stations, the *b*-values of the frequency–magnitude relationship for the aftershocks, and the 3D *P*-wave velocity model in and around the aftershock area.

We found that the mainshock consisted of two subevents propagating from south to north with focal mechanisms that are consistent with the surface rupture and the tectonic stress in the northern part of Sakhalin Island. Most of the aftershock activity occurred along the surface rupture, so it is generally consistent with the mainshock surface rupture and the focal mechanism. The *P*-wave velocity pattern was compared with the aftershock seismicity and the spatial distribution of the *b*-values, and our results suggest that high velocity correlates with high seismicity and small *b*-value.

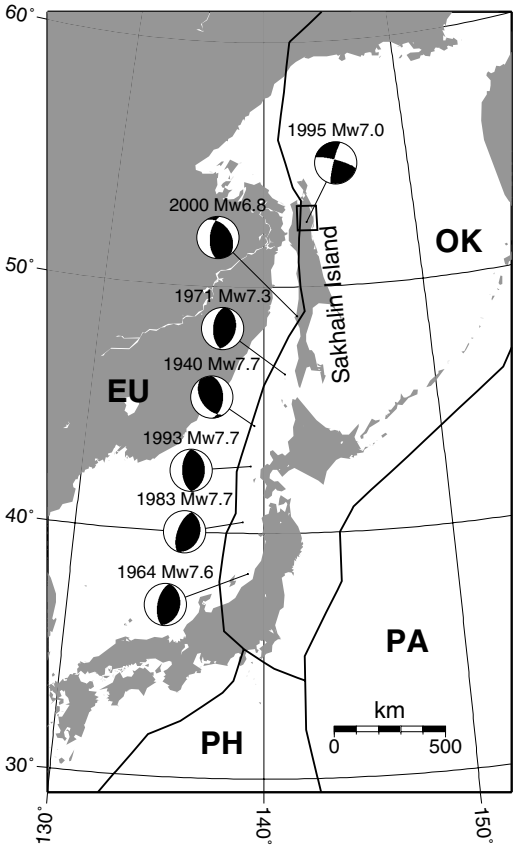

Figure 1. Tectonic map of the Sakhalin Island region and recent large earthquakes along the boundary between the Okhotsk plate (OK) and the Eurasian plate (EU). PA, Pacific plate; PH, Philippine Sea plate. Focal mechanisms were determined by Fukao and Furumoto (1975) (the events in 1940 and 1971), Hirasawa (1965) (the event in 1964), and Harvard University (the other events). The rectangle in the north of Sakhalin Island shows the study area where we deployed the temporary seismographic stations shown in Figure 5.

Source Process of the Mainshock

Data

The hypocentral parameters given by the U.S. Geological Survey (USGS) are origin time = 13:03:55.5 UT, epicenter = (52.534° N, 142.854° E), depth = 33 km, M_s 7.6, and m_b 6.6. We retrieved the broadband seismograms archived by the IRIS data center and chose the stations at distances between 30° and 90°, as shown in Table 1. The azimuthal coverage is good. We assumed the USGS source parameters and the J-B model (Jeffreys and Bullen, 1958) for the velocity model, calculated travel times, and discarded *P* and *S* waveform data for stations where the difference between the observed and calculated travel-time ($O - C$) values were larger than 5 sec. All the records were converted into ground-motion displacement with a sampling rate of 1 Hz.

Waveform Inversion

By careful inspection of recorded waveforms, two phases due to subevents were clearly identified several seconds after the arrival time of the *P* wave. We modeled these phases using two subevents with different mechanisms with the waveform inversion method of Kikuchi and Kanamori

Table 1
List of Seismographic Stations Used for the Waveform Inversion

Code	Azimuth (°)	Backazimuth (°)	Delta (°)	Components
AFI	134.9	−26.3	76.9	*P, SH*
ANMO	53.0	−36.2	74.0	*P*
ANTO	−50.3	37.5	69.8	*P, SH*
CCM	40.7	−30.2	78.2	*P, SH*
CHTO	−117.8	34.5	47.9	*P, SH*
CMB	60.2	−42.0	64.6	*P, SH*
COL	42.7	−75.8	36.0	*P*
COR	56.8	−45.5	58.3	*P, SH*
CTAO	176.6	−2.2	72.5	*P*
DPC	−33.7	31.9	67.9	*P*
ESK	−20.0	21.4	68.8	*P, SH*
FFC	37.1	−39.3	60.3	*P, SH*
GUMO	176.9	−2.0	39.0	*P*
HNR	161.1	−11.5	63.5	*P*
HRV	25.0	−20.4	80.7	*P, SH*
KBS	−11.8	40.2	45.5	*P, SH*
KEV	−24.3	46.2	49.4	*P, SH*
KONO	−24.8	30.2	61.9	*P*
PAS	61.5	−40.1	68.7	*P, SH*

(1993). Since the local velocity structure and the hypocenter depth significantly affect the waveform shapes, before the waveform inversion, we estimated the depth to the Moho and relocated the hypocenter using a trial-and-error method.

Depth to the Moho. The depth to the Moho affects waveforms for approximately 20 sec from the first motion. We calculated synthetic waveforms assuming a point source and the J-B model (Jeffreys and Bullen, 1958) for the velocity structure. This model includes an upper crust with a *P*-wave velocity of 5.57 km/sec and a thickness of 15 km and a lower crust of 6.50 km/sec and 18 km, so that the depth to the Moho is 33 km. For given values of *P*- and *S*-wave velocities and a fixed hypocenter depth of 9 km, the thickness of the crust was varied to fit the synthetics to the observations. We found that the data were best fit with a model where the upper and the lower crusts had thicknesses of 10 and 13 km, respectively, so that the depth to the Moho is 23 km. Figure 2a shows examples of the calculated and the observed waveforms.

Epicenter. We calculated *P*-wave arrival times assuming the J-B model (Jeffreys and Bullen, 1958) and the hypocenter determined by the USGS. The difference between the calculated and the observed arrival times was used to relocate the epicenter. With this relocation, the standard deviation of the $O - C$ values was reduced to 0.9 sec. We found that the redetermined epicenter (52.64° N, 142.83° E) corresponds, within 5 km, to the southern end of the surface fault (Shimamoto *et al.*, 1996) ruptured by this earthquake.

Centroid Depth. In order to estimate the centroid depth, we inverted waveforms assuming point sources with various depths and plotted the normalized residual error defined by

$$\bar{\Delta} = \frac{\sum_{j=1}^{N_s} \int \left[x_j(t) - y_j(t)\right]^2 dt}{\sum_{j=1}^{N_s} \int \left[x_j(t)\right]^2 dt},$$

where N_S is the number of seismograms used and $x_j(t)$ and $y_j(t)$ are observed and synthetic waveforms, respectively (Fig. 2b). Then we found that the centroid depth is 9 ± 3 km, with $\bar{\Delta}$ equal to 0.28 for 9 km. Taking into consideration the uncertainty in our knowledge of the velocity structure and ground noise levels, the difference of several percent in $\bar{\Delta}$ is not significant. Thus the centroid depth can range from 6 to 12 km.

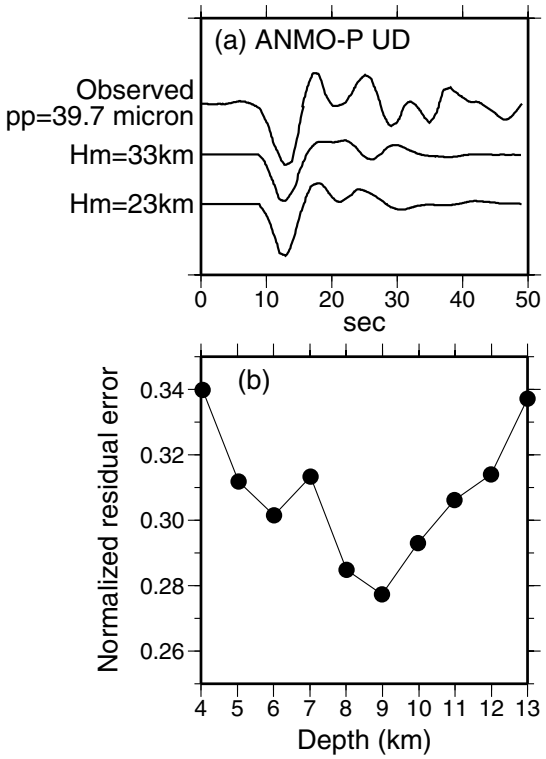

Figure 2. (a) Observed and synthetic waveforms assuming different depths to the Moho (H_m). The peak-to-peak amplitude (pp) is shown. (b) Waveform fit assuming different hypocentral depths of the mainshock.

Results of the Inversion

To determine the sequence of the two subevents, we used an iterative deconvolution method based on Kikuchi and Kanamori (1993) on a set of grid points at a depth of 9 km with equal spacing of 10 km on a horizontal line. The data set consisted of 31 body-wave records (vertical *P* and *SH* components). The mechanism was allowed to change during rupture, and the azimuth of the line on which the grid points were located was also an unknown parameter in the inversion. Figure 3a shows the mechanisms of two subevents and the source time functions that resulted from the inversion. Table 2 shows source parameters for the final solution. The waveforms matched very well at all stations, and $\bar{\Delta}$ was 0.27 (Fig. 4). Note that the two phases corresponding to the two subevents are clearly recorded on the *P* component at ANTO, DPC, ESK, KBS, and KEV. The first phase is small, and its duration is approximately 5 sec. The second phase follows immediately after the first one, and its amplitude is large. We interpreted the second phase as an *s*P wave rather than a direct *P* wave. For example, on the *P* component at KBS, the small first and large second phases were arrived at 5 and 10 sec from the beginning of the waveform, respectively.

Mechanism. The two subevents have almost the same mechanism, which is strike slip. Although the change in strikes of the two subevents is small, it is significant because a slight change in the strike results in a reversal of polarity of *SH* waves at stations close to the node; for example, see *SH* waves at CMB and PAS in Figure 4. The second subevent was located in a direction approximately N20°E from the first subevent. Thus the north–south nodal plane probably corresponds to the fault plane and the slip was right lateral. The focal mechanism we obtained is consistent with those determined by Harvard University and the USGS (Fig. 3b).

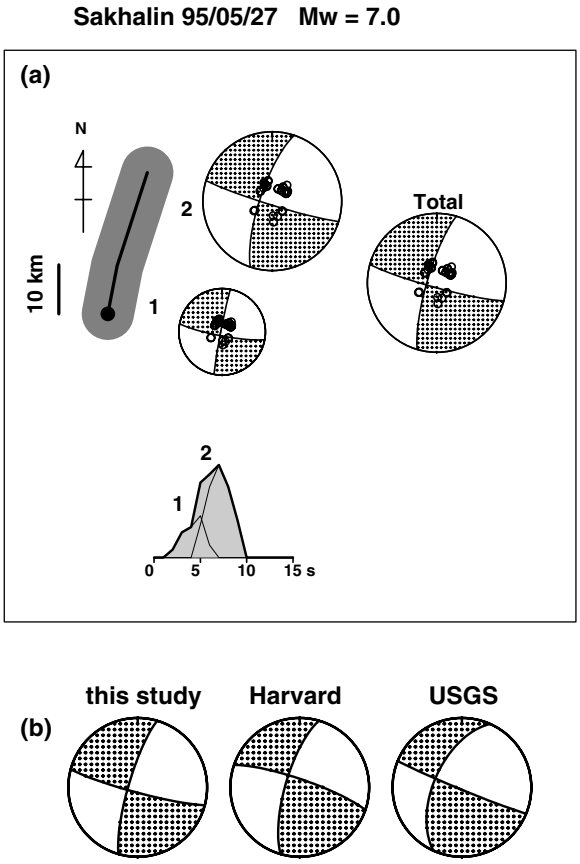

Figure 3. Focal mechanisms of the 1995 Sakhalin earthquake. (a) Mechanisms, locations, and moment rate functions for the two subevents and the whole earthquake. (b) Comparison of focal mechanisms from various studies.

Table 2
Focal Parameters Obtained by Waveform Inversion

Subevent	Mechanism (str,dip,slip)	Moment ($\times 10^{19}$ Nm)	Duration (sec)	D* (m)	$\Delta\sigma^{\dagger}$ (MPa)	Depth§ (km)
1	(191,87, −172)	1.2	0–6			
2	(198,76, −175)	3.1	3–9			
Total	(196,79, −174)	4.2	0–9	2.3	7	9

*Averaged displacement on the seismic fault.
†Stress drop.
§Depth of hypocenter.

Arefiev *et al.* (2000) obtained a source model with four subevents, which was more complicated than our model.

Length of the Mainshock Fault. From the waveform data, we estimate that the fault ruptured by the mainshock was 20–30 km long based on the following three points: (1) the second rupture extended over 20 km, which corresponds to two grid spacings of 10 km; (2) the first rupture initiated at the southern end of the fault and unilaterally propagated toward the north; and (3) the rupture duration time, that is, the rise time plus the rupture propagation time, was 9 sec. For rupture velocities of 2.5–3.5 km/sec, this gives fault lengths of 22.5–31.5 km. Our estimate of fault length is consistent with the observed length of the surface rupture, which was approximately 35 km (Shimamoto *et al.*, 1996). As described in a later part of this article, the length of the aftershock area was approximately 60 km, which was significantly longer than the lengths estimated from the waveform inversion and the surface rupture. Therefore we conclude that the length of the mainshock fault was constrained from 30 to 60 km.

Seismic Moment, Displacement, and Stress Drop. The seismic moment of the first subevent was one-third that of the second subevent. The total seismic moment was $M_0 = 4.2 \times 10^{19}$ N m, which, using the relation $\log_{10}M_0 = 1.5\ M_w + 9.1$ (Kanamori, 1977), gives M_w 7.0. Harvard University and USGS also estimated the moment magnitude as M_w 7.0. The length of fault L was estimated to be 30–60 km, as described in the previous section, and the width was 15 km based on the depth distribution of the aftershocks, as described in the following section. Then the area of fault is estimated to be $S = L \times W = 4.5$–9.0×10^8 m^2. Assuming that the rigidity μ is 3.0×10^{10} Pa, the averaged displacement is $D = M_0/\mu S = 1.6$–3.1 m. The stress drop is $\Delta\sigma = 2.5\ M_0/S^{1.5} = 4$–$11$ MPa, which is a representative value for intraplate events rather than interplate events at subduction zones.

Aftershock Activity

Temporary Seismic Observations

Using the results from a sparse survey from 7 to 10 June, immediately after the mainshock (Katsumata *et al.*, 1996), we deployed 12 temporary seismographic stations and monitored the aftershock activity from 10 June to 8 July 1995. Six stations were telemetered by radio to a central recording site, and the other six stations had local recording (Fig. 5 and Table 3).

Local Recording Seismic Stations. A local recording station consisted of a short-period L-28B seismometer (Mark Products), a DATAMARK LS-8000SH digital data recorder (Hakusan Industrial Corporation), and a rechargeable battery. The three-component L-28B had a natural frequency of 4.5 Hz, a coil resistance of 36 KΩ, and a sensitivity of 98.2 V/m/sec. For event recording, the DATAMARK has an event detection algorithm based on the monitoring of the ratio of the long-term to short-term averages of ground motion. The sampling frequency was 100 Hz. The DATAMARK has a GPS receiver to adjust the internal clock according to a timetable that a user specifies. We kept the accuracy of the internal clock within 10 msec by adjusting it every 6 hr. The GPS receiver was also used to obtain the station locations.

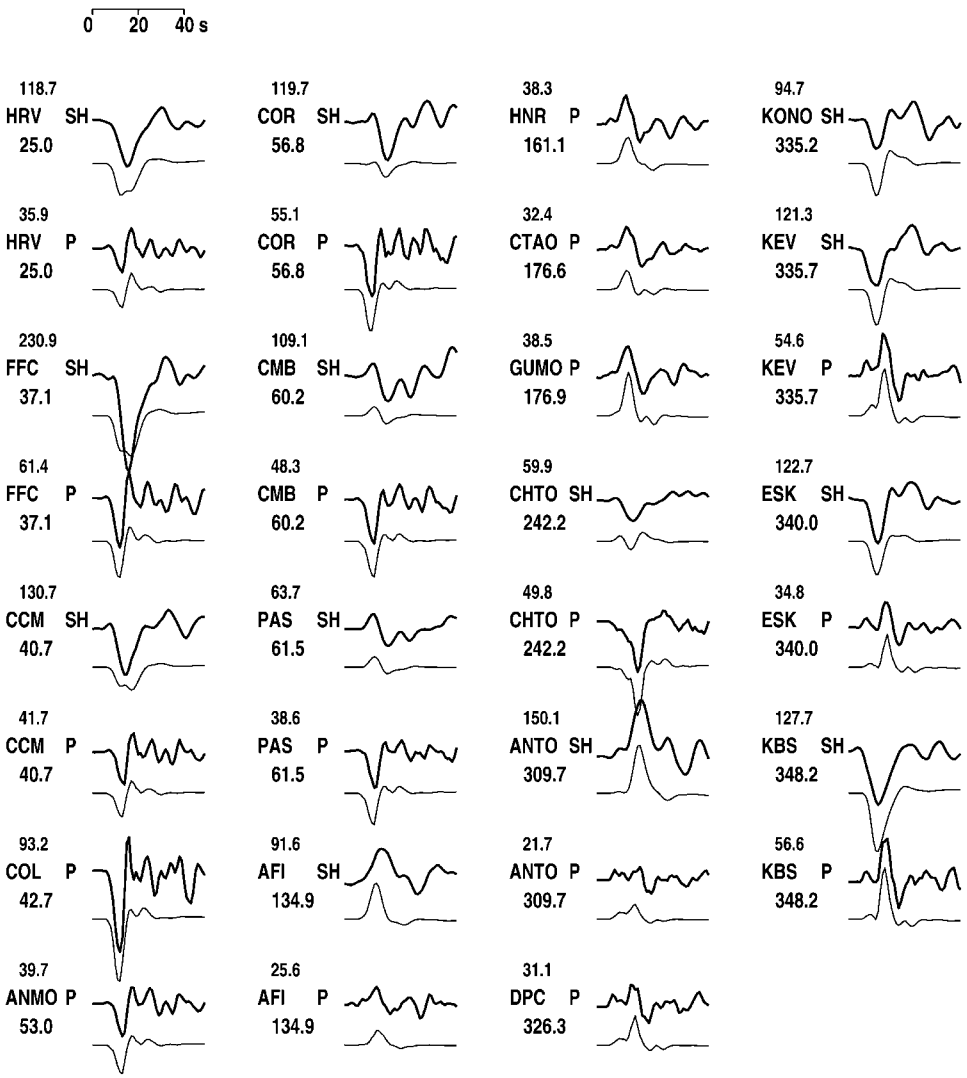

Figure 4. Observed (upper bold lines) and synthetic (lower thin lines) waveforms at each seismic station. The numbers above the station codes are peak-to-peak amplitudes of observed waveforms in microns, and the numbers below are the azimuths of the station from the earthquake.

Telemetered Seismic Stations. We also deployed six seismic stations telemetered by radio. Each station consisted of a three-component seismometer with a natural frequency of 1 Hz, a transmitter using radio waves in the 160-MHz band, and a battery to operate the system for 1 month. Waveform data from the six stations were received at our base camp in Sabo (CNT in Fig. 5), converted from analog to digital data using an IBM PC with a resolution of 12 bits, and stored on hard disks and digital audiotapes when events were detected. The clock for the telemetry system was corrected using GPS signals. The combination of the six telemetered and the six DATAMARK stations made up for the lack of station coverage that would result from using only one type of system. At the base camp in Sabo (CNT in Fig. 5), two seismometers were installed at the same site as a reference point for the telemetered and the DATAMARK networks.

Aftershock Distribution

We calculated hypocenters using the computer program HYPOMH (Hirata and Matsu'ura, 1987), which is based on a simple algorithm to find a maximum likelihood solution using a Bayesian approach. We assumed a 1D *P*-wave velocity model, as shown in Figure 6, and a Poisson's ratio of 0.25 in each layer. The model was based on seismic reflection surveys conducted by oil companies in Sakhalin. We located 2293 aftershocks from 10 June to 8 July 1995, and arrival times were picked at three or more seismic stations for almost all of the events (Fig. 7). Arefiev *et al.* (2000) also assumed a 1D *P*-wave velocity structure and calculated hypocenters of the aftershocks.

From the calculated aftershock locations, we found that most of the aftershocks occurred within the box labeled AB

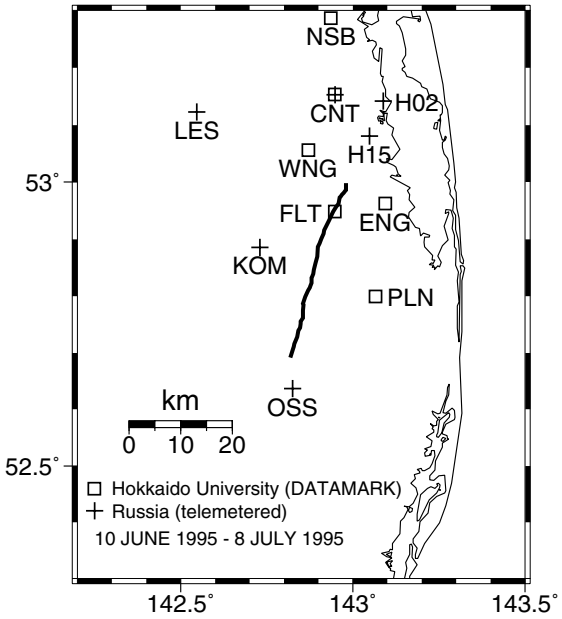

Figure 5. Temporary seismographic stations deployed between 10 June and 8 July 1995. The bold line indicates the surface trace of the fault (Shimamoto *et al.*, 1996).

Table 3
List of Temporary Seismographic Stations Deployed between 10 June and 8 July 1995

Code	Latitude (°N)	Longitude (°E)	Height (m)	Recorder
CNT	53.1533	142.9485	90	Telemeter, DATAMARK
PLN	52.7998	143.0660		DATAMARK
ENG	52.9625	143.0940		DATAMARK
FLT	52.9488	142.9470		DATAMARK
WNG	53.0560	142.8708		DATAMARK
NSB	53.2863	142.9362		DATAMARK
H02	53.1415	143.0885	20	Telemeter
H15	53.0807	143.0490	155	Telemeter
KOM	52.8853	142.7293	150	Telemeter
OSS	52.6373	142.8250	390	Telemeter
LES	53.1230	142.5472	30	Telemeter
VAL*	52.3765	143.0648		DATAMARK
PLT*	52.7555	143.0767		DATAMARK

*Seismic stations used only for a preliminary survey from 7 to 10 June.

in Figure 8a. The aftershock area is approximately 60 km long, which is significantly longer than the surface rupture. The western part of the aftershock area bounded by the surface rupture included more epicenters than the eastern part. This is consistent with our result from the waveform inversion that showed one of the nodal planes dipping toward the west. The statistical location errors in the horizontal directions are smaller than 1 km in the northern part of the aftershock area and larger than 5 km in the southern part. The density of seismic stations causes the difference in the location error.

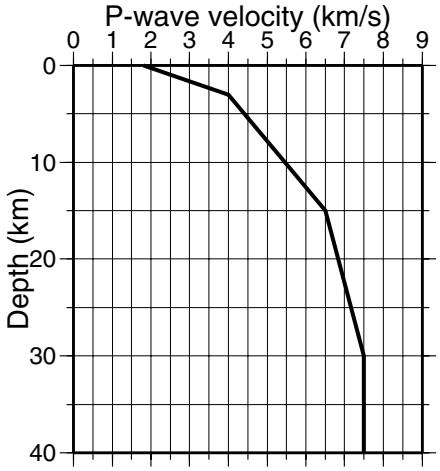

Figure 6. *P*-wave velocity model used in the location of the aftershocks. Poisson's ratio is assumed to be 0.25 in each layer.

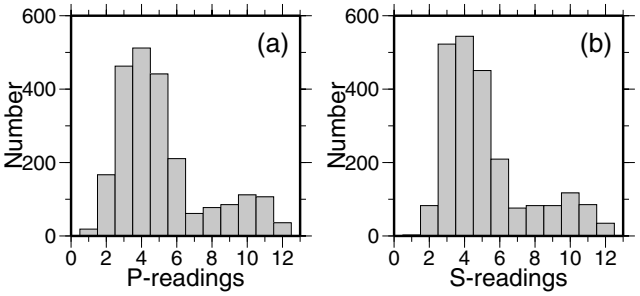

Figure 7. Number of arrival-time readings used in this study: (a) *P* wave and (b) *S* wave.

A cross section along the surface rupture shows that hypocenters are distributed between 5 and 15 km in depth in the northern part (Fig. 8b). The statistical location error is approximately 2 km in depth. Few aftershocks seemed to occur shallower than 5 km. Although most of the aftershocks are located to be shallower than 5 km in the southern part, this is not reliable because the statistical location error is large.

Figure 9 shows the aftershock distribution for several depth ranges. Eighty percent of the aftershocks occurred from 4 to 12 km in depth (Fig. 9, panels 4–6 km to 10–12 km). There are five areas with high seismicity: (1) around the epicenter of the mainshock; (2) around (52.8° N, 142.8° E) at 6–10 km depths, that is, the central part of the surface rupture; (3) around (53.0° N, 142.9° E) at 10–12 km depths, that is, the northern end of the surface rupture; (4) around (53.1° N, 142.9° E) at 8–10 km depths, that is, around the seismic station WNG; and (5) around (53.0° N, 142.7° E) at 4–8 km depths in region C in Figure 8a. The cluster in region C was activated after the largest aftershock with *M* 5.0 on June 13 (Fig. 10).

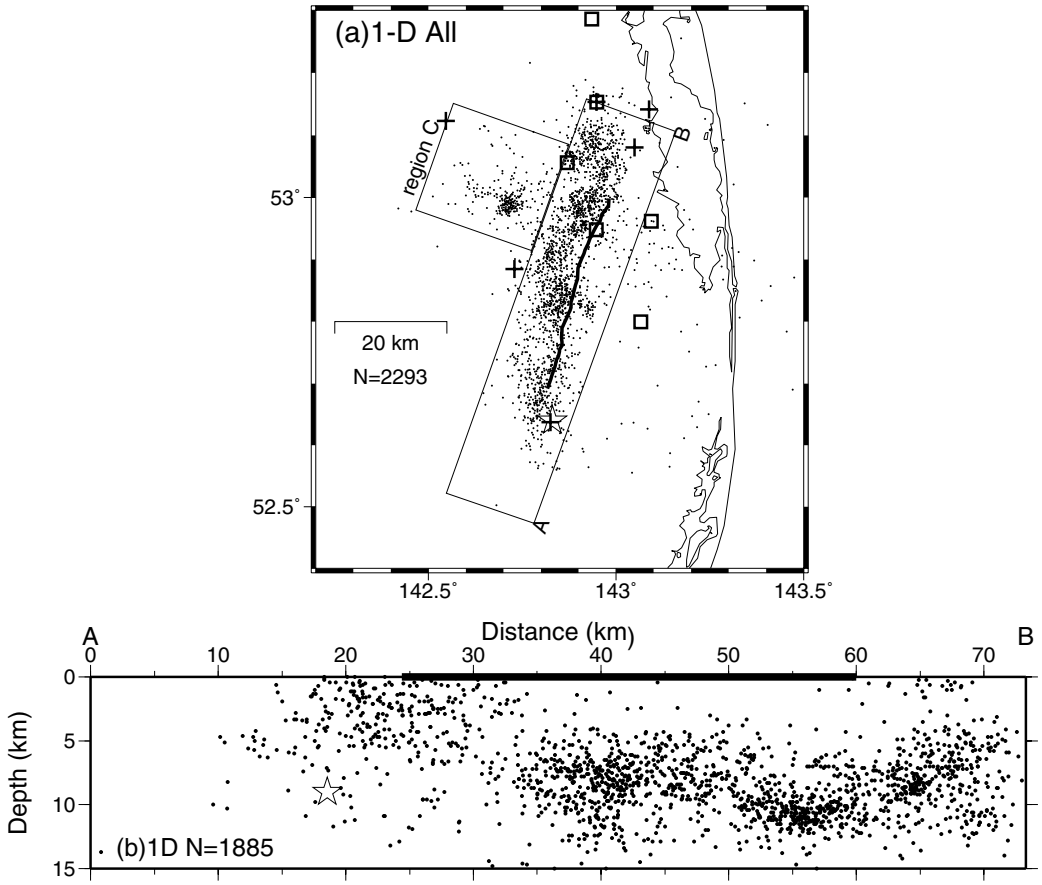

Figure 8. Epicenters of 2293 aftershocks of the 1995 Sakhalin earthquake for the time period from 10 June to 8 July 1995. The events were located with the 1D *P*-wave velocity model in Figure 6 and a Poisson's ratio of 0.25. (a) Epicenters and (b) a vertical cross section along AB in (a). The open star indicates the epicenter of the mainshock obtained from the waveform analysis in this study. The bold line is the surface trace of the fault ruptured by the mainshock. Rectangles and crosses indicate the temporary seismographic stations shown in Figure 5.

b-Value Mapping

The frequency–magnitude distribution (Ishimoto and Iida, 1939; Gutenberg and Richter, 1944) is one of the reliable empirical relations in seismology; it represents the frequency of occurrence of earthquakes as a function of magnitude:

$$\log_{10} N = a - bM,$$

where N is the cumulative number of earthquakes with magnitudes larger than M and a and b are constants. There are some explanations for different b-values: (1) high and low stresses cause earthquakes with small and large b-values, respectively (Scholz, 1968; Wyss, 1973; Urbanic *et al.*, 1992); and (2) material heterogeneity (Mogi, 1962) and thermal gradients (Warren and Latham, 1970) also can cause a change in b-values. As for an interesting observation related to the rupture process, Wiemer and Katsumata (1999) found that aftershocks have large b-values in areas that had large slip during the mainshock.

Data and Method

We used the 2293 hypocentral data obtained using the 1D velocity model with the computer program ZMAP (Wiemer and Wyss, 1997) to make a b-value map for the aftershocks recorded in 1995. Since the method is described in Wiemer and Wyss (1997), we only give an outline of the analysis. First we plotted the number of earthquakes versus magnitude in the aftershock area to estimate the magnitude of completeness, M_C (Fig. 11a). We concluded that all aftershocks with M 2.1 and larger were detected and located by our temporary seismographic network, that is, M_C 2.1. The aftershock area was divided into grids with spacings of 0.01° in latitude and longitude. A circle was drawn around each grid point, and its radius was increased until it included $N = 100$ aftershocks with magnitude $M = M_C$ or larger. The b-value was calculated for the selected 100 aftershocks, and the grid point was colored according to the b-value.

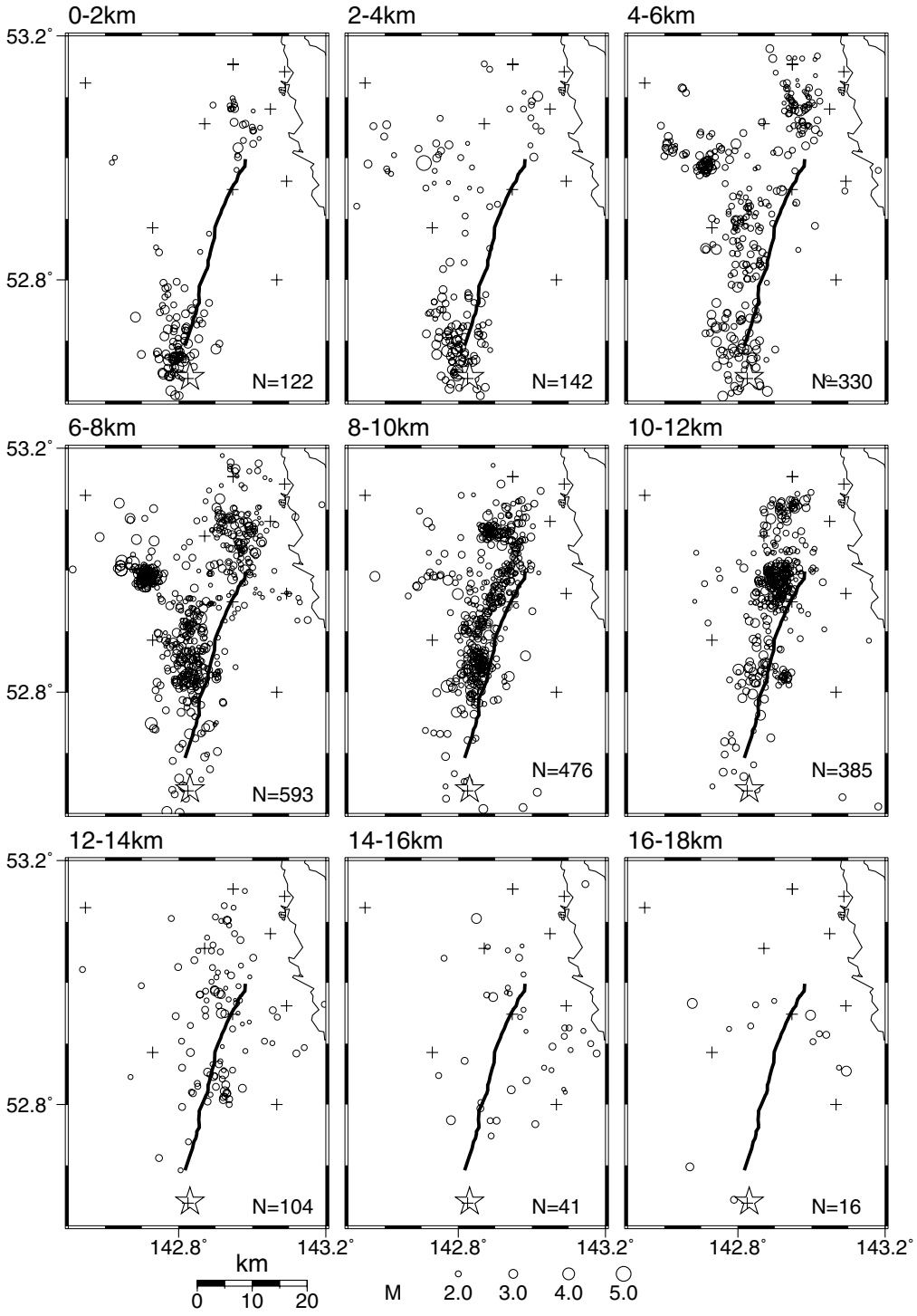

Figure 9. Similar to Figure 8, with the epicenters in different depth ranges identified by the numbers on the top of each panel. *N* is the number of events.

Results

Region C and the central part of the aftershock area were associated with small *b*-values (blue in Fig. 12). Areas with large *b*-values (red in Fig. 12) were imaged around the southern and the northern parts of the aftershock area. For instance, the *b*-value at a grid point in region C (circle A in Fig. 12) was 0.7, and at a grid point in the southern part of the aftershock area (circle B) the *b*-value was 1.5. In order to evaluate the significance of the values, the probability that two samples may come from the same population was calculated (Utsu, 1992). In this case the probability was very

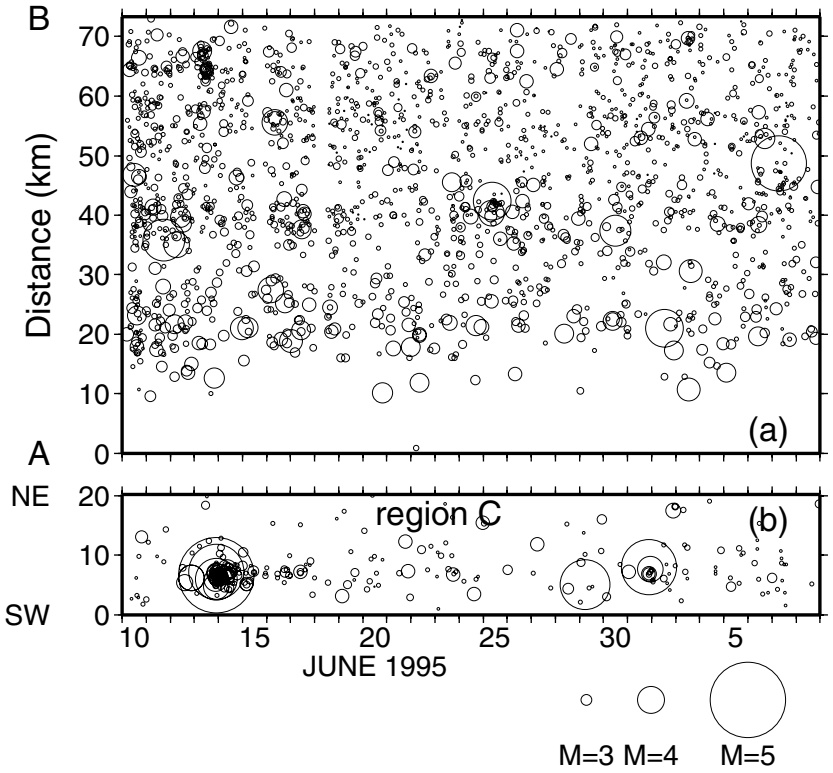

Figure 10. Space-time plots for the aftershock activity using the 1D hypocenter catalog (a) along AB in Figure 8 and (b) in region C. Times are in UT.

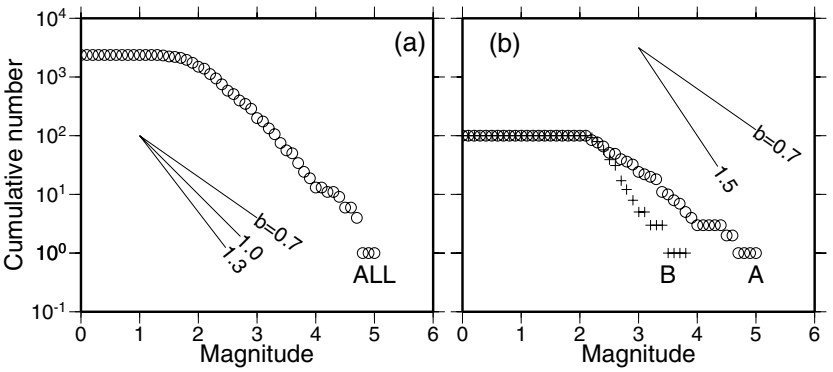

Figure 11. Magnitude–frequency relation for the aftershocks of the 1995 Sakhalin earthquake. The *b*-value denotes the slope of the relation. (a) Plot for all the aftershocks located and (b) plot for areas labeled A and B in Figure 12.

small, 0.0000021. Therefore these two *b*-values were significantly different from each other (Fig. 11b).

Three-Dimensional *P*-Wave Velocity Structure

Data and Method

The seismic stations in Figure 5 were used for the determination of 3D *P*-wave velocity structure in the focal area of the 1995 Sakhalin earthquake. We selected a total of 872 aftershocks that were recorded well by at least five stations and had stable locations with root mean square less than 0.25 sec (Fig. 13a). This selection gave 6036 *P*-wave arrival-time observations. The accuracy for most of the arrival times is considered to be around 0.05 sec.

We divided the focal area (52.3–53.4° N, 142.2–143.5° E) into 13 × 9 horizontal grid spacing with dimensions of approximately 7 km in the central area and 14 km in the surrounding area (Fig. 14). In the depth direction, five grids points were placed at 0, 5, 10, 15, and 20 km from the ground surface. We used the computer program SIMULPS12 developed by Thurber (1983, 1993) to analyze the selected arrival times. Unknown parameters for the inversion were hypocentral parameters, station corrections, and the *P*-wave velocity at the grid nodes. We assumed a starting *P*-wave velocity model for the inversion, shown in Table 4, which was based on the velocity model in Figure 6 used for the 1D hypocenter location. At the grids in the surrounding area, we fixed *P*-wave velocity to the initial value, and the velocity was inverted at only the grids in the central area.

Station corrections for *P* waves were included in the 3D inversion. The station corrections are very small: 0.01 sec at CNT, 0.03 sec at PLN, 0.19 sec at ENG, −0.08 sec at FLT, −0.17 sec at WNG, 0.10 sec at NSB, 0.11 sec at H02, −0.04

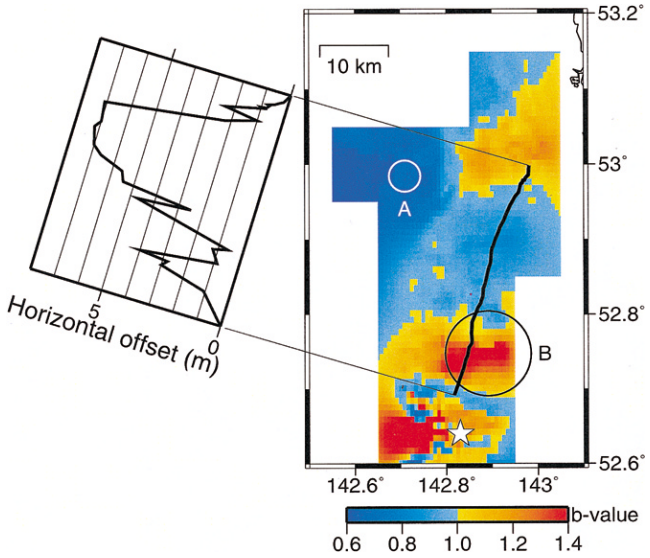

Figure 12. The *b*-value map for aftershocks of the 1995 Sakhalin earthquake and the horizontal offset of the surface rupture measured by Shimamoto *et al.* (1996). The aftershocks were located using the 1D velocity model of Figure 6. The open star indicates the epicenter of the mainshock obtained from the waveform analysis in this study.

sec at H15, −0.10 sec at KOM, and −0.06 sec at OSS. The solution is obtained by iterative, damped least-squares method. The damping parameter for the *P*-wave velocity was determined by a trade-off curve (Eberhart-Phillips, 1986) (Fig. 15a). In this case, we used 13 for the inversion. In each iteration the maximum *P*-wave velocity adjustment was 0.15 km/sec. The inversion significantly improved the fit to the data in three iterations, as evaluated with an *F*-test (Fig. 15b). The reduction in data variance was 34% from the initial model. The epicenters were relocated well and the distribution became tighter after the inversion (Fig. 13b).

Results

The *P*-wave velocity images of the focal area of the 1995 Sakhalin earthquake are shown in plan view for 5, 10, and 15 km depth in Figure 16. Perturbations from the initial model are indicated in percent. Red and blue portions correspond to low and high velocities, respectively. The diagonal elements of the resolution matrix are also shown in Figure 16 for each depth. The resolution is very poor in the southern part of the study area and to the west of 142.85° E. At 5 km depth the *P*-wave velocity ranges from −8.6% to +8.6%, that is, from 4.80 to 5.70 km/sec. The slowest and the fastest grids were located at (53.0° N, 142.9° E) and (52.9° N, 142.9° E), respectively. The low-velocity areas are imaged around the northern end and east of the surface trace of the fault, which seem to surround the high-velocity area around the central part of the surface trace. At 10 km depth the *P*-wave velocity ranges from −8.0% to +8.6%, that is, from 4.83 to 5.70 km/sec. The low-velocity area is limited to the northern part of the study area, and the high-velocity area covers almost all over the aftershock zone along the surface trace. At 15 km depth the northern part of the surface trace seems to remain in the high-velocity area.

Discussion and Conclusion

Our discussion will focus on five major aspects of our work.

1. Correlation between aftershock seismicity patterns and *P*-wave velocity patterns. Some previous studies have found good correlations between aftershock activity and seismic velocity structure. Most aftershocks occurred in the high-velocity anomalies of *P* waves for the 1986 North Palm Springs earthquake (Nicholson and Lees, 1992), the 1989 Loma Prieta earthquake (Lees, 1990), the 1992 Landers earthquake (Zhao and Kanamori, 1993), and the 1994 Northridge earthquake (Zhao and Kanamori, 1995). All of these earthquakes occurred in a region of California where there is a typical continental plate boundary shear zone. On the other hand, most aftershocks occurred in the low-velocity anomaly of *P* wave for the 1995 Hyogoken-Nanbu (Kobe) earthquake in Japan (Zhao *et al.*, 1996), which is located close to a typical subduction zone. For the 1995 Sakhalin earthquake, the aftershocks appear to occur in the high-velocity area rather than the low-velocity area.
2. Correlation between velocity patterns and *b*-value patterns. Comparing the *b*-value map in Figure 12 with the *P*-wave velocity perturbation at a depth of 10 km in Figure 16b, we found a correlation between velocities and the *b*-values. The *b*-values are relatively small for the aftershocks located in areas of high velocities.

   Because there are no volcanoes or geothermal activity that may cause dense fractures and thermal gradients in the crust in and around the aftershock area, probably only the stress controls the *b*-values. As noted before, regions where the stress level is high and low produce seismicity with small and large *b*-values, respectively (Scholz, 1968; Wyss, 1973; Urbanic *et al.*, 1992). The correlation between velocity patterns and *b*-value patterns suggests that the shear stress level was relatively higher in the high-velocity regions as a result of fault motions of the Sakhalin mainshock. This interpretation is at odds with the fact that the postseismic stress averaging all over the focal area should be lower than the stress before the mainshock occurred. Spatial heterogeneity in elasticity may cause the difference in the state of postseismic stress.
3. Correlation between *b*-value patterns and slip patterns at the mainshock. Wiemer and Katsumata (1999) pointed out that the *b*-values for aftershocks are controlled by the amount of slip on a fault during a mainshock. Since the slip distribution on the fault of the 1995 Sakhalin earthquake was not determined, we were not able to compare

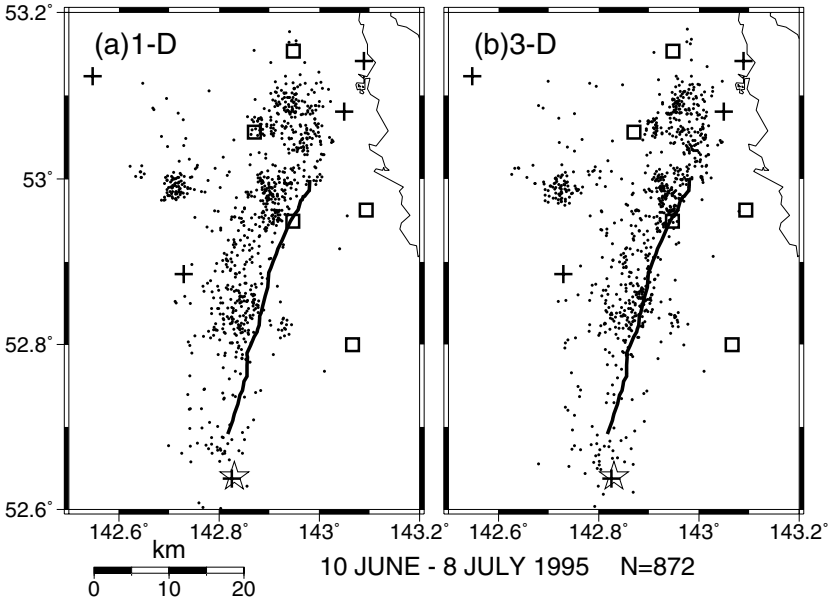

Figure 13. Aftershock relocation for the 1995 Sakhalin earthquake for the time period from 10 June to 8 July 1995. The 3D *P*-wave velocity model, hypocenters, and station corrections were determined simultaneously. (a) Epicenters before relocation using the 1D *P*-wave velocity model in Figure 6. (b) Epicenters after the simultaneous inversion. Other symbols are same as in Figure 8.

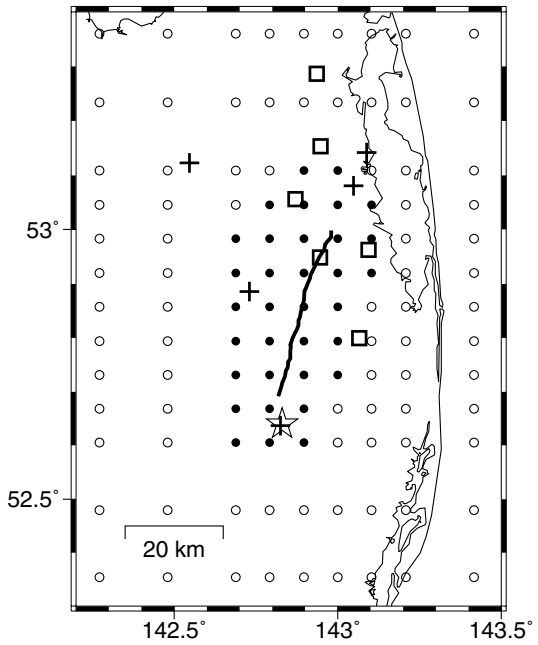

Figure 14. Grid points for 3D *P*-wave velocity inversion. Velocity is fixed to the initial value at the points shown by open circles. Other symbols are as in Figure 8.

Table 4
1D Initial *P*-Wave Velocity Model for the 3D Velocity Inversion

Depth (km)	Velocity (km/sec)
0	3.00
5	5.25
10	5.25
15	7.00
20	7.00

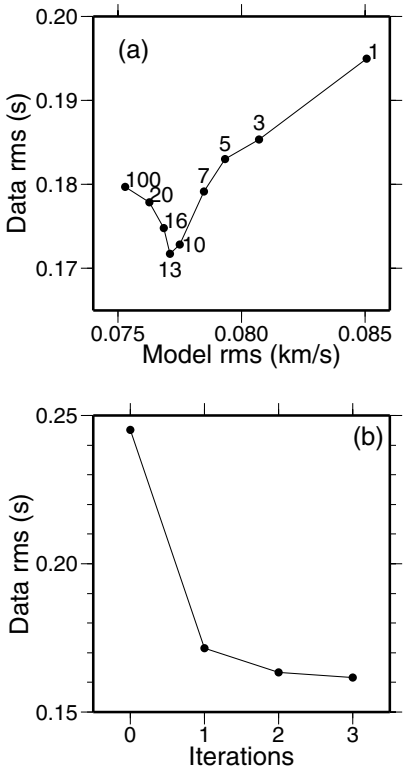

Figure 15. (a) Trade-off curve for selecting optimal damping value. Root mean square (rms) of the data and that of the model are computed after one iteration for the indicated damping value (adjacent to symbols). A value of 13 was used in this case. (b) The data rms after each iteration.

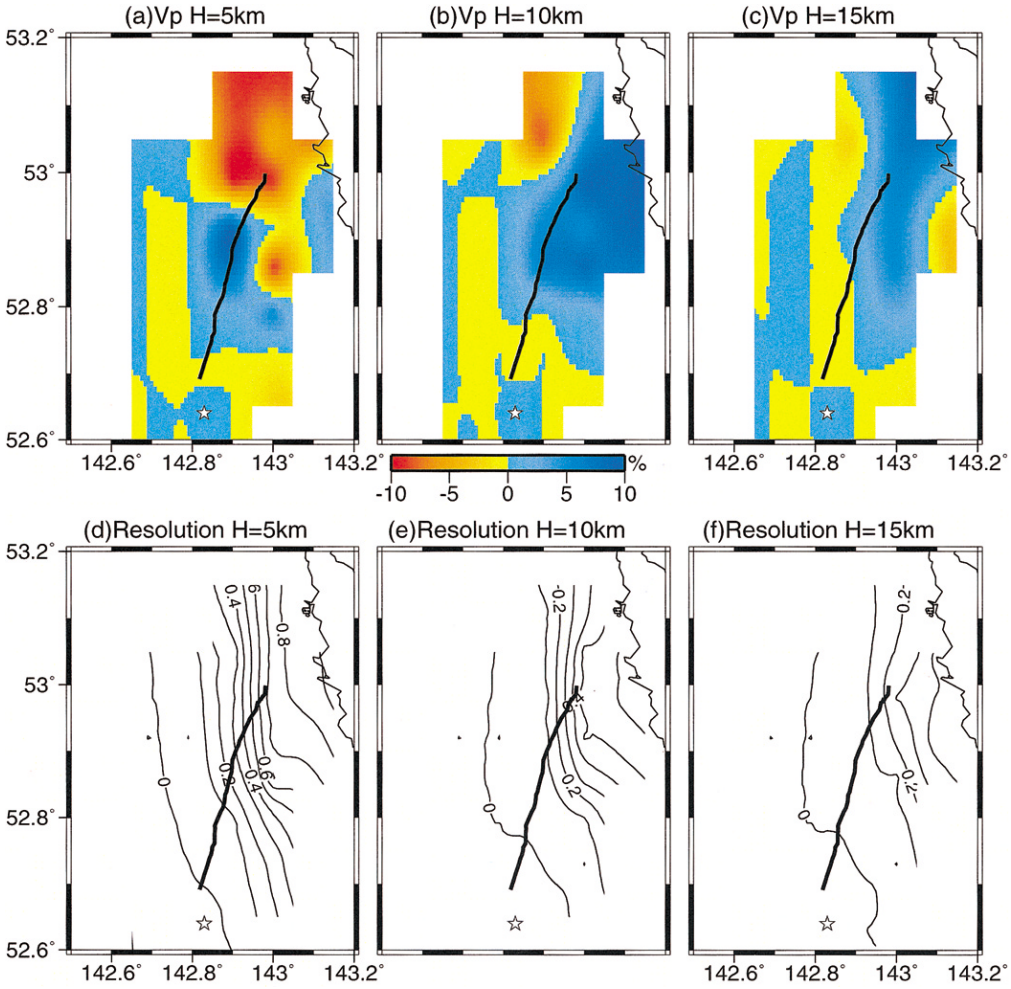

Figure 16. 3D *P*-wave velocity model for the focal area of the 1995 Sakhalin earthquake. Velocity perturbations are shown in percent at depths of (a) 5 km, (b) 10 km, and (c) 15 km. The perturbations are measured from the initial velocity in Table 4. Negative (red) and positive (blue) perturbations correspond to low and high velocities, respectively. The bold line indicates the surface trace of the fault. The open star indicates the epicenter of the mainshock obtained from the waveform analysis in this study. (d)–(f) Resolution at each depth. The contour interval is 0.1.

the *b*-value pattern with the slip pattern as Wiemer and Katsumata (1999) did. However we can estimate it as follows.

Shimamoto *et al.* (1996) measured the offset on the surface rupture of the Sakhalin earthquake and found two peaks: one located in the southern part with a small slip and the other in the northern part with a large slip (Fig. 12). We found in the present study that the mainshock consisted of two subevents: a small one in the southern part and a large one in the northern part (Fig. 3). Therefore the slip on the fault was probably larger in the northern part than the southern part. In that case the aftershocks have small *b*-values in areas that had large slip during the mainshock, which seems to be inconsistent with the hypothesis proposed by Wiemer and Katsumata (1999).

4. Aftershock activity in 1996 and 1997. In 1996 and 1997 we conducted temporary seismic observations in the focal area. We found that the aftershock activity continued for at least 2 years after the mainshock.

The temporary observations in 1996 started on 3 August and ended on 18 August. Six seismic stations were deployed around the northern end of the surface rupture. We used the DATAMARK system as described in a previous section. In this period we located 134 earthquakes. The pattern of epicenters was found to be almost the same as that in 1995. Activity continued in some clusters along the AB section in Figure 7. In region C no seismicity was detected.

The temporary observations in 1997 started on 3 August and ended on 11 August. Ten seismic stations were deployed around the aftershock area. We used the DATAMARK system at five stations and a digital audio tape recorder system at five stations. In this period we located 167 microearthquakes.

5. Plate boundary. Seismicity is the primary basis for identifying the plate boundary. From this point of view, the 1995 Sakhalin earthquake should be one of the outstanding events that define the plate boundary. Although there were relatively many shallow microearthquakes on Sakhalin Island and the north–south–trending seismic belt was identified before the 1995 event, it was not obvious whether the seismic belt was definitely the plate boundary because no large earthquake was recorded historically. After the occurrence of the 1995 event, we are more confident of the Sakhalin plate boundary model.

   The focal mechanism of the mainshock of the 1995 event was different from other events in the seismic belt. The 1995 event was a strike-slip event, and the others were reverse-fault events (see Fig. 1). Seno *et al.* (1996) showed that the Okhotsk plate can be discriminated from the North American plate and that its Euler pole is located around the northern Sakhalin Island. The direction of Eurasia–Okhotsk relative motion at the center of the surface faulting of the 1995 event (52.90° N 142.91° E) (Takahashi *et al.*, 1995) is predicted to be N14°E, which is consistent with the slip vector N6°E obtained by the waveform inversion in this study and the N15°E surface faulting (Suzuki *et al.*, 1995). If the 1995 Sakhalin earthquake occurred to the east of the Eurasia–Okhotsk pole, it would be on a transform fault. The other thrust-type earthquakes to the south would represent Eurasia–Okhotsk convergence. Seno *et al.*'s interpretation seems to be the most plausible to explain the change in focal mechanism.

In conclusion, the source process of the mainshock and the aftershock distribution are the most important information to understand the dynamics and the tectonic meaning of large earthquakes. Although we should remember that the Sakhalin earthquake in 1995 caused severe damage, it was useful to gain an understanding of the tectonics in the northern part of Sakhalin Island. In this article we found that the mainshock consisted of two subevents with focal mechanisms that indicated almost the same right-lateral strike-slip faulting. About 2000 events were located in an aftershock area of 60 km × 10 km trending in a N15°E direction, which is consistent with the surface rupture.

Acknowledgments

We thank James Mori of Kyoto University for improving the English of the manuscript. We also thank Cliff Thurber and Donna Eberhart-Phillips for the SIMULPS12 program and Stefan Wiemer for the ZMAP program. Comments from Max Wyss, an anonymous reviewer, and Jose Pujol were helpful to revise the manuscript. The GMT software (Wessel and Smith, 1991) was used to process and map data. The present study was supported by the Ministry of Education, Science, Culture, and Sports of Japan (Grant Number 07300009).

References

Arefiev, S., E. Rogozhin, R. Tatevossian, L. Rivera, and A. Cisternas (2000). The Neftegorsk (Sakhalin Island) 1995 earthquake: a rare interplate event, *Geophys. J. Int.* **143,** 595–607.

Chapman, M. E., and S. C. Solomon (1976). North American–Eurasian plate boundary in northeast Asia, *J. Geophys. Res.* **81,** 921–930.

Eberhart-Phillips, D. (1986). Three-dimensional velocity structure in northern California coast ranges from inversion of local earthquake arrival times, *Bull. Seism. Soc. Am.* **76,** 1025–1052.

Fukao, Y., and M. Furumoto (1975). Mechanisms of large earthquakes along the eastern margin of the Japan Sea, *Tectonophysics* **26,** 247–266.

Fournier, M., L. Jolivet, P. Huchon, K. F. Sergeyev, and L. S. Oscorbin (1994). Neogene strike-slip faulting in Sakhalin and the Japan Sea opening, *J. Geophys. Res.* **99,** 2701–2725.

Gutenberg, R., and C. F. Richter (1944). Frequency of earthquakes in California, *Bull. Seism. Soc. Am.* **34,** 185–188.

Hirasawa, T. (1965). Source mechanism of the Niigata earthquake of June 16, 1964, as derived from body waves, *J. Phys. Earth* **13,** 35–66.

Hirata, N., and M. Matsu'ura (1987). Maximum-likelihood estimation of hypocenter with origin time eliminated using nonlinear inversion technique, *Phys. Earth Planet. Interiors* **47,** 50–61.

Ishimoto, M., and K. Iida (1939). Observations of earthquakes registered with the microseimograph constructed recently, *Bull. Earthquake Res. Inst. Tokyo Univ.* **17,** 443–478.

Ivashchenko, A. I., C. Kim, and G. A. Bondarenko (1990). Seismicity of shallow earthquakes in the Okhotsk Sea, in *Seismic Zoning of Shelves*, A. I. Ivashchenko (Editor), Far-East Division of Russian Academy of Sciences, Vladivostok, 22–37 (in Russian).

Jeffreys, H., and K. E. Bullen (1958). Seismological tables, Office of the British Association, Burlington House, London.

Kanamori, H. (1977). The energy release in great earthquakes, *J. Geophys. Res.* **82,** 2981–2987.

Katsumata, K., M. Kasahara, S. Sen, C. Kim, S. Sergey, A. Ivaschenko, R. Tatevossian, S. Lukyanenko, K. Pletnev, and V. Strakhov (1996). Japan–Russia joint observation of aftershocks of the 1995 Sakhalin earthquake (in Japanese), *Geophys. Bull. Hokkaido Univ.* **59,** 177–188.

Kikuchi, M., and H. Kanamori (1993). Source complexity of the 1988 Armenian earthquake: evidence for a slow after-slip event, *J. Geophys. Res.* **98,** 15,797–15,808.

Kim, C. (1990). On the problem of definition of potential earthquake source zones within the north Sakhalin onshore and offshore areas, in *Seismic Zoning of Shelves*, A. I. Ivashchenko (Editor), Far-East Division of Russian Academy of Sciences, Vladivostok, 99–116 (in Russian).

Kim, C., and G. A. Bondarenko (1990). An estimate of maximum magnitude of earthquakes in the north-east Sakhalin island, in *Seismic Zoning of Shelves*, A. I. Ivashchenko (Editor), Far-East Division of Russian Academy of Sciences, Vladivostok, 117–129 (in Russian).

Lees, J. M. (1990). Tomographic *P*-wave velocity images of the Loma Prieta earthquake asperity, *Geophys. Res. Lett.* **17,** 1433–1436.

Mogi, K. (1962). Magnitude–frequency relation for elastic shocks accompanying fractures of various materials and some related problems in earthquakes, *Bull. Earthquake Res. Inst. Tokyo Univ.* **40,** 831–853.

Nicholson, C., and J. M. Lees (1992). Travel-time tomography in the northern Coachella Valley using aftershocks of the 1986 M_L 5.9 North Palm Springs earthquake, *Geophys. Res. Lett.* **19,** 1–4.

Scholz, C. H. (1968). The magnitude–frequency relation of microfracturing in rock and its relation to earthquake, *Bull. Seism. Soc. Am.* **58,** 399–415.

Seno, T., T. Sakurai, and S. Stein (1996). Can the Okhotsk plate be discriminated from the North American plate? *J. Geophys. Res.* **101,** 11,305–11,315.

Shimamoto, T., M. Watanabe, Y. Suzuki, A. Kozhurin, M. Strel'tsov, and E. Rogozhin (1996). Surface faults and damage associated with the

1995 Neftegorsk earthquake, *J. Geol. Soc. Japan* **102,** 894–907 (in Japanese).

Solov'yev, S. L. (1965). Seismicity of Sakhalin, *Bull. Earthquake Res. Inst. Tokyo Univ*. **43,** 95.

Suzuki, Y., M. Watanabe, T. Shimamoto, A. I. Kozhurin, and M. I. Strelizhov (1995). Maximum offset along the Nefchegorsk earthquake fault (in Japanese), *Abstr. Seismol. Soc. Japan* **2,** 57.

Takahashi, H., M. Kasahara, N. Vasilenko, A. Ivashchenko, C. U. Kim, F. Kimata, and T. Seno (1995). Coseismic deformation around the northern part of epicentral area of the 1995 North Sakhalin earthquake deduced from geodetic observations, Russia's federal system of seismological networks and earthquake prediction, information and analytical bulletin, 121–126.

Thurber, C. H. (1983). Earthquake locations and three-dimensional velocity structure in the Coyote Lake area, central California, *J. Geophys. Res.* **88,** 8226–8236.

Thurber, C. H. (1993). Local earthquake tomography: velocities and v_P/v_S—theory, in *Seismic Tomography: Theory and Practice*, H. M. Iyer and K. Hirahara (Editors), Chapman and Hall, London, 563–583.

Tobita, M., S. Fujiwara, S. Ozawa, P. A. Rosen, E. J. Fielding, C. L. Werner, Mas. Murakami, H. Nakagawa, K. Nitta, and Mak. Murakami (1998). Deformation of the 1995 North Sakhalin earthquake detected by JERS-1/SAR interferometry, *Earth Planets Space* **50,** 313–325.

Urbanic, T. I., C. I. Trifu, J. M. Long, and R. P. Toung (1992). Space–time correlations of *b* values with stress release, *Pure Appl. Geophys.* **139,** 449–462.

Utsu, T. (1992). On seismicity, in *Report of the Joint Research Institute for Statistical Mathematics*, *Inst. for Stat. Math., Tokyo* 139–157.

Warren, N. W., and G. V. Latham (1970). An experimental study of thermally induced microfracturing and its relation to volcanic seismicity, *J. Geophys. Res.* **75,** 4455–4464.

Wessel, P., and W. H. F. Smith (1991). Free software helps map and display data, *EOS* **72,** 441, 445–446.

Wiemer, S., and K. Katsumata (1999). Spatial variability of seismicity parameters in aftershock zones, *J. Geophys. Res.* **104,** 13,135–13,151.

Wiemer, S., and M. Wyss (1997). Mapping the frequency–magnitude distribution in asperities: an improved technique to calculate recurrence time? *J. Geophys. Res.* **102,** 15,115–15,128.

Wyss, M. (1973). Towards a physical understanding of the earthquake frequency distribution, *Geophys. J. R. Astr. Soc.* **31,** 341–359.

Zanyukov, V. N. (1971). The central Sakhalin fault and its role in the tectonic evolution of the island, *Dokl. Akad. Nauk SSSR*, **196,** 85 (English translation).

Zhao, D., and H. Kanamori (1993). The 1992 Landers earthquake sequence: earthquake occurrence and structural heterogeneities, *Geophys. Res. Lett.* **20,** 1083–1086.

Zhao, D., and H. Kanamori (1995). The 1994 Northridge earthquake: 3-D crustal structure in the rupture zone and its relation to the aftershock locations and mechanisms, *Geophys. Res. Lett.* **22,** 763–766.

Zhao, D., H. Kanamori, H. Negishi, and D. Wiens (1996). Tomography of the source area of the 1995 Kobe earthquake: evidence for fluids at the hypocenter? *Science* **274,** 1891–1894.

Institute of Seismology and Volcanology
Hokkaido University
Sapporo 060-0810, Japan
(K.K., M.Ka., M.I.)

Earthquake Research Institute
University of Tokyo
Tokyo 113-0032, Japan
(M.Ki.)

Institute of Marine Geology and Geophysics
Russian Academy of Science
Yuzhno-Sakhalinsk, Russia
(C.-U.K., A.I.)

Institute of Physics of the Earth
Russian Academy of Science
123810 Moscow, B. Gruzinskaya 10, Russia
(R.T.)

Manuscript received 14 August 2002.